Polyhedron 153 (2018) 173–180

Contents lists available at ScienceDirect

Polyhedron

journal homepage: www.elsevier.com/locate/poly

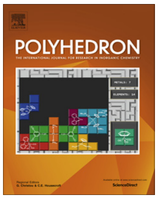

Two new alkaline earth metal organic frameworks with the diamino derivative of biphenyl-4,4′-dicarboxylate as bridging ligand: Structures, fluorescence and quenching by gas phase aldehydes

Stavros A. Diamantis [a], Anastasia D. Pournara [b], Antonios G. Hatzidimitriou [a], Manolis J. Manos [b], Giannis S. Papaefstathiou [c], Theodore Lazarides [a,*]

[a] Department of Chemistry, Aristotle University of Thessaloniki, 54124 Thessaloniki, Greece
[b] Department of Chemistry, University of Ioannina, Dourouti Campus, 45500 Ioannina, Greece
[c] Laboratory of Inorganic Chemistry, Department of Chemistry, National and Kapodistrian University of Athens, Panepistimiopolis, Zografou 15771, Greece

A R T I C L E I N F O

Article history:
Received 30 March 2018
Accepted 9 July 2018

Dedicated to Professor Spyros Perlepes on the occasion of his 65th birthday.

Keywords:
Metal organic frameworks
Alkaline earths
Fluorescence
Aldehydes
Sensors

A B S T R A C T

Alkaline earth metal ion organic frameworks (AEMOFs) represent a relatively underexplored subcategory of MOFs. Two new MOFs $[Ca_6(bpdc\text{-}(NH_2)_2)_5(\mu_3\text{-}HCO_2)_2(H_2O)_{2.5}(DMF)_{0.5}]\cdot 0.5H_2O\cdot 2.5DMF$ (**1**) and $[Sr_4(bpdc\text{-}(NH_2)_4)(\mu_2\text{-}DMF)_2(DMF)_{1/3}]\cdot 2/3(DMF)$ (**2**) [$H_2bpdc\text{-}(NH_2)_2$ = 2,2′-diamino-[1,1′-biphenyl]-4,4′-dicarboxylic acid); DMF = N,N-dimethylformamide] are presented here. These MOFs display structural variety with diverse topologies and new structural features. Luminescence studies revealed that both MOFs display ligand based fluorescence with small differences in emission profiles possibly attributable to the difference in charge density of the metal ions combined with the different conformation adopted by the ligand in the crystal structures of **1** and **2**. Furthermore, initial sensing studies reveal that both MOFs can potentially function as fluorescent sensors for gas phase aldehydes.

1. Introduction

Metal organic frameworks (MOFs) or Porous Coordination Polymers (PCPs) are a class of hybrid crystalline materials, assembled by metal ions or clusters and bridging polydentate organic ligands to form polymeric network structures containing potential voids [1–3]. Due to their properties such as structural and functional diversity, porosity, high surface area, and adsorption affinity towards various guest species, MOFs have been used for a variety of applications including gas storage and separation [4–10], catalysis [11–13], ion exchange [14–20], and proton conduction [21]. One more important advantage of MOFs is the facile introduction of interesting physical properties such as luminescence through the use of photoactive ligands, metal ions or their combinations. Thus, luminescent MOFs (LMOFs), represent an important rapidly growing subcategory of MOFs [22]. These luminescent crystalline materials show great prospects in a range of technological applications from phosphors in lighting devices [23–28], photocatalysts [29–34], luminescent molecular thermometers [35–37], biomedical imaging [38–42] and luminescent sensors [14,20,43–49].

Alkaline earth metal-based MOFs (AEMOFs) are still relatively rare in comparison to their transition metal and rare earth based counterparts. Nevertheless, AEMOFs display unique advantages over transition and lanthanide-based MOFs such as: (i) low cost because of the high natural abundance of alkaline earths, (ii) reduced toxicity, (iii) low density of the early members of the alkaline earth series which is an important property for gas storage applications and (iv) stability in air and various solvents. Despite the fact that the research on AEMOFs remains on a rather preliminary level, AEMOFs exhibit interesting properties and they have been used in several applications [50–62]. Recently, our group reported a series of AEMOFs based on the bridging ligand 2,5-dihydroxy terephthalate, which exhibits unusual luminescence properties because of excited state intramolecular proton transfer (ESIPT). The ESIPT process has been shown to be partly hindered due to electrostatic repulsion between the mobile proton and the coordinated alkaline earth ion with the lighter ions inducing a more pronounced effect as a result of their higher charge density [63,64]. Among the AEMOFs studied by our group, a Mg^{2+} based MOF can

---

* Corresponding author.
E-mail address: tlazarides@chem.auth.gr (T. Lazarides).

https://doi.org/10.1016/j.poly.2018.07.010
0277-5387/

be used for real time detection of water traces in organic solvents via an “turn on” luminescence sensing mechanism [63].

In this contribution, we present two new alkaline earth metal ion MOFs, namely $[Ca_6(bpdc\text{-}(NH_2)_2)_5(\mu\text{-}HCO_2)_2(H_2O)_{2.5}(DMF)_{0.5}]\cdot 0.5H_2O\cdot 2.5DMF$ (**1**) and $[Sr_4(bpdc\text{-}(NH_2)_4)(\mu\text{-}DMF)_2(DMF)_{1/3}]\cdot 2/3DMF$ (**2**). The compounds display structural diversity forming three dimensional frameworks with different secondary building units (SBUs) [65] and network topologies. These AEMOFs exhibit bright blue fluorescence following population of the ligand based $^1\pi\pi^*$ and $^1n\pi^*$ excited states. Furthermore, the presence of free amino groups which are possibly able to react with carbonyl compounds in the frameworks of **1** and **2** prompted us to study their fluorescence properties in the presence of gas phase aldehydes. Indeed, preliminary studies revealed that both MOFs display significant fluorescence quenching upon their exposure to vapors of volatile aldehydes thereby showing potential as gas phase aldehyde sensors.

2. Experimental part

2.1. Materials and methods

All starting materials and solvents were used as received from the usual commercial sources (Sigma Aldrich, Alfa Aesar and TCI).

2.2. Physical methods

Thermogravimetric analysis (TGA) data were recorded on a Mettler-Toledo TGA/DSC1 instrument. Thermal analysis was conducted from 25 to 800 °C under a N_2 atmosphere (50 mL min^{-1}) with a heating rate of 5 °C min^{-1}. The ^1H NMR spectra of the ligand were recorded at room temperature and on Agilent 500 MHz instrument, with the use of the solvent proton as an internal standard. PXRD patterns were recorded on a Bruker D8 Advance X-ray diffractometer with Cu-Kα radiation (λ = 1.5418 Å). IR spectra were recorded on KBr pellets in the 4000–400 cm^{-1} range using a PerkinElmer Fourier Transform IR spectrophotometer. The UV–vis spectra in solution were recorded on a Hitachi-2001 spectrophotometer in the wavelength range of 200–500 nm while UV–vis diffuse reflectance spectra were obtained at room temperature on a Shimadzu 1200 PC spectrophotometer in the wavelength range of 200–800 nm. $BaSO_4$ powder was used both as a reference (100% reflectance) and a base material on which the powder sample was coated. The reflectance data were converted to absorption using the Kubelka-Munk function. The fluorescence spectra were measured on a Hitachi F-7000 spectrofluorometer equipped with a red sensitive Hamamatsu R928 photomultiplier tube detector. Appropriate long pass filters were used to remove scattering from the sample and the monochromators.

2.3. Single-crystal X-ray crystallography

Single crystals of the MOFs were obtained from reaction mixtures according to the described synthetic procedures. For the structural determination of **1** and **2**, single crystals of the respective MOF were mounted on a Bruker Kappa APEX II diffractometer, equipped with a triumph monochromator at ambient temperature. Diffraction measurements were recorded using MoKα radiation. The data were collected at 130 K over a full sphere of reciprocal space. Intensity data were collected using φ and ω scan mode. The frames collected for each crystal were integrated with the Bruker SAINT software package [66] using a narrow-frame algorithm. Data were corrected for absorption using the numerical method (SADABS) based on crystal dimensions [67]. The powder X-ray diffraction (PXRD) data of **1** and **2** show excellent agreement with the simulated PXRD patterns of the compounds (Fig. S1 and Fig. S2 respectively) thereby confirming that the analyzed single crystals are representative of the bulk samples.

All structures were solved using the SUPERFLIP [68] package and were refined by the full-matrix least-squares method on F^2 using the CRYSTALS package version 14.40b [69]. All non-hydrogen atoms have been refined anisotropically except in the case of disordered atoms.

All hydrogen atoms were found at their expected positions and refined using soft constraints. By the end of the refinement, they were positioned using riding constraints. CCDC 1833862–1833863 contain the supplementary crystallographic data for this paper. These data can be obtained free of charge via www.ccdc.cam.ac.uk/data_request/cif. The crystal data, details of data collection and structure refinement for both MOFs are given in Table 1. Illustrations were drawn by the Mercury program [70]. Further details on the crystallographic studies as well as atomic displacement parameters are given as Supporting Information in the form of cif files.

2.4. Compound preparation

2.4.1. Synthesis of $H_2bpdc\text{-}(NH_2)_2$

Dimethyl-2,2′-dinitro-[1,1′-biphenyl]-4,4′-dicarboxylate. Dimethyl-biphenyl-4,4́-dicarboxylate (1.00 g, 3.7 mmol) was added into concentrated H_2SO_4 (10 mL). The mixture was stirred at room temperature for 10 min. Nitric acid (760 μL, 3 eq.) was added into concentrated H_2SO_4 (2 mL). This solution was added dropwise into the first mixture at room temperature over a period of 20 min. The mixture was stirred at room temperature for 4 h and then poured into ice (300 mL) to form a beige solid. The resulting solid was dissolved in dichloromethane and the aqueous phase was extracted with dichloromethane (3 × 70 mL). The combined organic layers were dried over Na_2SO_4 and evaporated under reduced pressure to afford a beige solid. The crude mixture was recrystallized from 2-propanol and washed with diethyl ether to give the pure product. Yield: 1.2 g (3.33 mmol, 90%). ^1H NMR (500 MHz, $CDCl_3$): δ (ppm): 8.90 (s, 2H), 8.37 (d, J = 8.4 Hz, 2H), 7.40 (d, J = 8 Hz, 2H), 4.02 (s, 6H).

Dimethyl-2,2′-diamino-[1,1′-biphenyl]-4,4′-dicarboxylate. Dimethyl-2,2′-dinitro-[1,1′-biphenyl]-4,4′-dicarboxylate (1.2 g, 3.33 mmol) was dissolved in 20 mL acetic acid and the solution was stirred under Ar for 10 min. To this solution iron powder (3.7 g, 10 eq.) was added and the mixture was stirred at room

Table 1
Selected crystal data for **1** and **2**.

Compound	**1**	**2**
Chemical formula	$C_{81}H_{77}Ca_6N_{13}O_{30}$	$C_{75}H_{81}Sr_4N_{13}O_{21}$
Formula mass	1953.05	1851.02
Crystal system	monoclinic	monoclinic
a (Å)	13.782(3)	12.4481 (16)
b (Å)	30.575 (7)	25.930 (4)
c (Å)	11.112 (2)	13.2612 (19)
α (°)	90	90
β (°)	105.628 (7)	109.292 (4)
γ (°)	90	90
Unit Cell Vol (Å^3)	4509.1 (17)	4040.1 (10)
Temperature (K)	130	130
Space group	$P2_1/c$	$P2_1/c$
Z	2	2
No. of reflections measured	50527	56760
No. of independent reflections	8284	7749
No of observed reflections [$I > 2.0\sigma(I)$]	5984	5646
R_{int}	0.028	0.053
$R[F^2 > 2\sigma(F^2)]$	0.038	0.047
$wR(F^2)$	0.090	0.086

temperature for 24 h. The suspension was filtered through Celite, washed with 40 mL acetic acid and the filtrate was concentrated under reduced pressure. The solid was dissolved in ethyl acetate (80 mL) and was extracted with saturated aqueous sodium carbonate solution (2 × 80 mL) and H_2O (3 × 80 mL). The combined organic layers were dried over Na_2SO_4 and the solution was evaporated under vacuum to yield the product as a yellow solid. Yield 900 mg (3 mmol, 90%). ^{1}H NMR (500 MHz, DMSO d_6): δ (ppm): 7.42 (s, 2H), 7.21 (d, J = 7.8 Hz, 2H), 7.06 (d, J = 7.8 Hz, 2H), 4.97 (s, 4H), 3.81 (s, 6H).

2,2′-Diamino-[1,1′-biphenyl]-4,4′-dicarboxylic acid H_2bpdc-$(NH_2)_2$. Dimethyl 2,2′-diamino-[1,1′-biphenyl]-4,4′-dicarboxylate (900 mg, 3.0 mmol) was dissolved in THF (20 mL) and 20 mL of aqueous NaOH (0.6 M) were added dropwise under vigorous stirring. The mixture was stirred overnight at room temperature. The organic solvent was removed under vacuum and the aqueous solution was acidified with acetic acid to yield a light brown solid (735 mg, 2.7 mmol, 90%). ^{1}H NMR (500 MHz, DMSO d_6): δ (ppm) = 12.64 (br, 2H), 7.40 (s, 2H), 7.20 (d, J = 7.6 Hz, 2H), 7.40 (d, J = 7.8 Hz, 2H), 4.90 (br, 4H).

*2.4.2. Synthesis of MOFs **1** and **2***

*$[Ca_6(bpdc\text{-}(NH_2)_2)_5(\mu_3\text{-}HCO_2)_2(H_2O)_{2.5}(DMF)_{0.5}]\cdot 0.5\ H_2O\cdot 2.5DMF$ (**1**).* $CaCl_2$ (6.4 mg, 0.058 mmol) was added as a solid into a solution of H_2bpdc-$(NH_2)_2$ (15.0 mg, 0.055 mmol) in 3 mL DMF/H_2O (9:1 v/v), in a Teflon cup. The mixture was sonicated at room temperature for *ca.* 3 min and then, the Teflon cup was transferred into a 23 mL stainless steel autoclave. The autoclave was sealed and placed in an oven at 120 °C, remained undisturbed at this temperature for 24 h and was then cooled to room temperature. Plate-like brown crystals of **1** were isolated by filtration, washed with DMF and dried under vacuum for 20 h. Yield 13.0 mg (~61%). IR (KBr pellets, cm^{-1}): 3426 m, 3360 m, 2920 w, 2850 w, 1669 m, 1654 m, 1638 m, 1629 m, 1590 s, 1541 s, 1534 s, 1432 s, 1394 s, 1358 m, 1317 w, 1287 w, 1250 w, 1147 w, 1111 w, 1089 w, 1008 w, 938 w, 899 w, 780 m, 679 m.

*$Sr_4(bpdc\text{-}(NH_2)_4)(\mu_2\text{-}DMF)_2(DMF)_{1/3}]\cdot 2/3\ (DMF)$ (**2**).* $Sr(NO_3)_2$ (11.7 mg, 0.055 mg) was added as solid into a solution of H_2-bpdc-$(NH_2)_2$ (15.0 mg, 0.055 mmol) in 3 mL DMF/H_2O (9:1 v/v), in a Teflon cup. The procedure followed was identical to that for the synthesis of MOF **1**. Prism-like brown crystals of **2** were isolated by filtration, washed with DMF and dried under vacuum for 20 h. Yield: 12.0 mg (~47%). IR (KBr pellets, cm^{-1}): 3436 m, 3336 m, 3208 w, 2923 w, 1654 m, 1648 m, 1583 m, 1540 s, 1487 w, 1422 w, 1392 s, 1321 w, 1275 w, 1256 w, 1143 w, 1105 w, 1001 w, 909 w, 805 m, 780 m.

3. Results and discussion

3.1. Description of structures

*Crystal Structure of **1**.* Single-crystal X-ray diffraction analysis reveals that **1** crystallizes in the monoclinic $P2_1/c$ space group (Table 1). As seen in Fig. 1, the framework of **1** features of an infinite rod SBU which consists of a $Ca_3(COO)_5(\mu_3\text{-}HCO_2)(H_2O)_{1.5}(DMF)_{0.5}$ repeating unit and comprises three crystallographically independent coordinated Ca^{2+} ions (i.e., Ca1, Ca2 and Ca3) and three crystallographically independent bridging bpdc-$(NH_2)_2^{2-}$ dicarboxylate ligands (i.e., L_1, L_2 and L_3). The Ca1 ion is seven-coordinated by seven oxygen atoms to form a distorted face capped octahedron in which four oxygen atoms are from the carboxylate groups of L_1 and L_2 ligands, one formate oxygen (O12) originating from DMF hydrolysis, one coordinated water molecule (O13), and another oxygen (O14) which was modeled as originating from a coordinated water molecule and from the C═O group of a coordinated terminal DMF molecule (50% occupancy). The Ca2 and Ca3 ions are also seven-coordinated by oxygen atoms and each of them is ligated with six carboxylate groups which belong to three different ligands and one μ_3-η^1:η^2:η^2 bridging formate oxygen (O11). The geometries around Ca2 and Ca3 ion are best described as distorted face capped octahedral and distorted pentagonal bipyramidale respectively. Furthermore, the coordinated water molecule (O13) forms strong hydrogen bonds (1.9–2.5 Å) with neighboring oxygen and nitrogen moieties (O1, N5, N7). If all DMF (coordinated and guest molecules) were removed from the structure the solvent-accessible volume calculated by Mercury would be approximately 7.4% of the unit cell volume. Selected bond lengths and bond angles for **1** are listed in Table S1.

From the topological view, the Ca^{2+} ions along with the carboxylates and the formate anions form a zig-zag chain (rod) along the *c* crystallographic axis (Fig. 2A). By taking under account that the carboxylate C atoms (C1, C14, C15, C28 and C29) are the connection points along the rod, a ladder is created along *c* which is composed by edge and face sharing square pyramids (Fig. 2B–E). These ladders are connected through ligands L_1 and L_2 to create a 2D layer parallel to the *ac* plane (Fig. 2F). Finally, the layers are connected through the third ligand (L_3) along *b* to create a 3D network

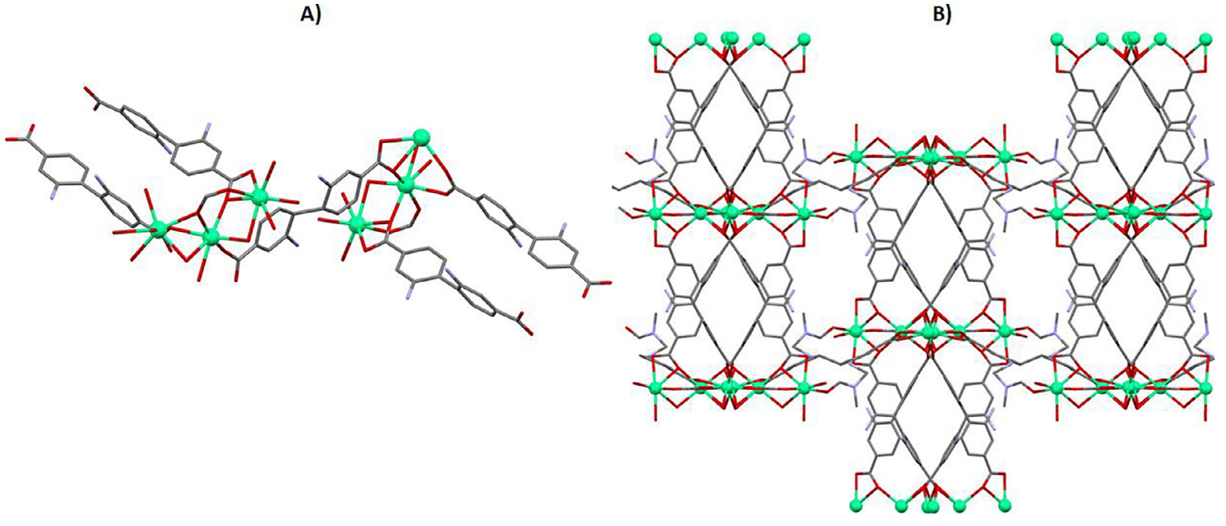

Fig. 1. Representation of the (a) infinite SBU and (b) 3-D structure along the c axis of **1**.

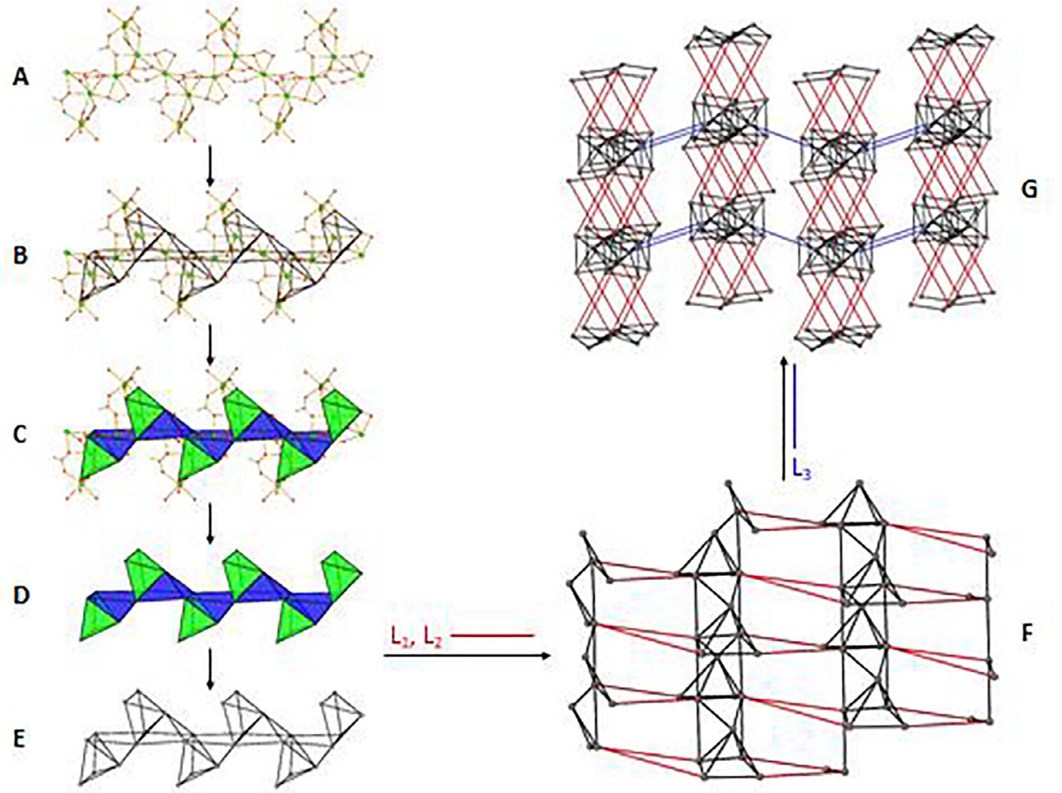

Fig. 2. The deconstruction of the framework of **1**. Color code: Ca green, C grey, O red, H cyan, L_1 and L_2 red, L_3 blue. (Colour online.)

(Fig. 2G). The resulting unique tri-nodal network comprises one type of 4-coordinated and two types 7-coordinated nodes with stoichiometry $(4\text{-c})_2(7\text{-c})_2(7\text{-c})$ and has a point symbol of $(3^2.4^2.5.6)_2(3^5.4^6.5^4.6^6)_2\{3^7.4^6.5^2.8^6)$.

*Crystal structure of **2**.* MOF **2** crystallizes in the monoclinic space group $P2_1/n$ and displays a three dimensional framework. The structure of **2** is based on an infinite rod SBU which consists of a $[Sr_2(COO)_4(\mu\text{-DMF})_2(DMF)]$ unit in which there are two crystallographically unique Sr^{2+} ions (Sr1 and Sr2). Sr1 is eight coordinated, and is ligated to six carboxylate oxygen atoms and two μ_2-DMF ligands (Fig. 3). On the other hand the Sr2 ion is nine coordinated, and its coordination sphere contains six carboxylate oxygen atoms, two oxygen atoms originating from two bringing DMF molecules and an oxygen atom (O11) originating from a disordered terminal DMF ligand (one third of which was modeled as coordinated and two thirds as a lattice DMF molecule in a general position). It should be noted that the amino groups of each dicarboxylic ligand from intraligand hydrogen bonds (~3.0 Å). The terminal DMF ligands are situated inside the cavities of the MOF (Fig. 3B). Ignoring them, the solvent accessible void of **2** calculated by MERCURY is ~10.7% of the unit cell volume. Selected bond lengths and bond angles for **2** are listed in Table S2.

Topologically, the Sr^{2+} ions along with the carboxylates groups and the bridging DMF molecules form a chain (rod) along the 1 0 1 vector (Fig. S3A). By taking under account that the carboxylate C atoms (C1, C14, C15 and C28) are the connection points along the rod, a ladder is created (Fig. S3B–D). These ladders are connected through bridging ligands to create a uninodal, 4-coordinated **sra** 3D network (Fig. 3C) with point symbol $(4^2.6^3.8)$. The same **sra** rod-net has been found in MOF-69 [71], MOF-71 [72] and MIL47/MIL53/MIL60 [2,73].

3.2. Thermal stability

The thermal stability of **1** and **2** was studied by thermogravimetric analysis (TGA) under N_2 atmosphere. The thermograph of **1** is shown in Fig. 4 with red line. The weight loss was observed in three steps. In the first step (100–170 °C) we observe weight loss of the coordinated and guest water molecules (experimental loss of 2.85%, theoretically estimated loss of 2.77%). The second stage of

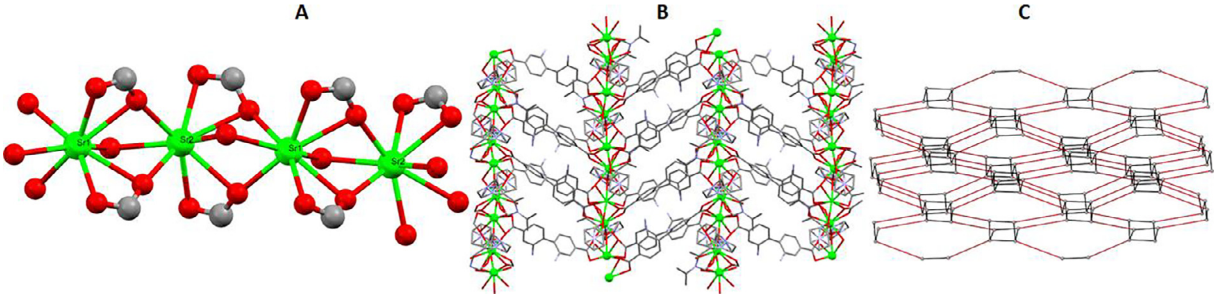

Fig. 3. Representation of the (a) SBU and (b) 3-D structure along the *a* axis (c) **sra** network of **2**. H atoms and solvent molecules were omitted for clarity. Color code: Sr, green; C, gray; O, red; N, blue. (Colour online.)

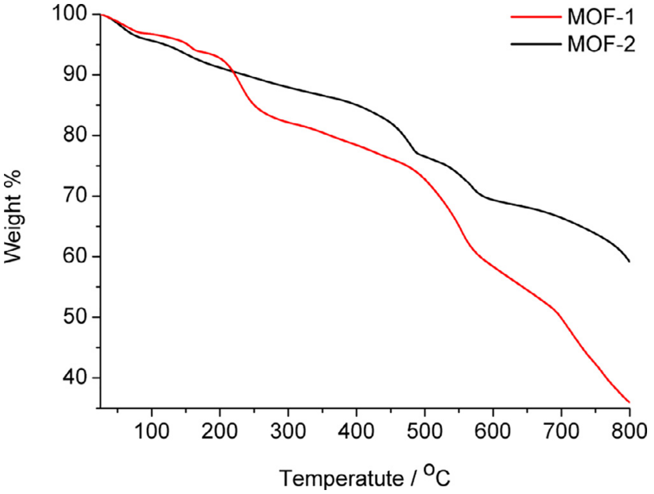

Fig. 4. The TGA curves for MOFs **1** and **2** (red and black line respectively). (Colour online.)

thermal decomposition begins at 170 °C and ends at 290 °C and includes the possible loss of the coordinated and guest DMF molecules (experimental loss of 11.35%, theoretically estimated loss of 11.25%), followed by decomposition of the framework up to 800 °C. In the case of **2** shown with black line the weight loss was observed at two discreet steps. The first weight loss (100–420 °C) corresponds to the removal of three coordinated and guest DMF molecules (experimental loss of 11.65%, theoretically estimated loss of 11.84%) before decomposition of the framework sets in.

3.3. Photoluminescence properties

The luminescence properties of MOFs **1** and **2** were studied in the solid state at room temperature. As shown in Fig. S4 the H_2-bpdc-$(NH_2)_2$ ligand displays turquoise fluorescence in methanol with emission maximum at 475 nm (λ_{exc} = 330 nm). The emission is likely derived from the radiative decay of spin allowed $^1\pi\pi^*$ and $^1n\pi^*$ excited states (250 and 330 nm respectively) the latter involving the lone pair of the amino group (Fig. S5). Upon excitation at 350 nm, **1** and **2** exhibit blue-shifted emission (Fig. 5A) in comparison to the free ligand (**1**: λ_{em} = 445 nm; **2**: λ_{em} = 464 nm). Based on the electronic configurations of Ca^{2+} and Sr^{2+} ions and the similarity of the emission spectra to that of the free ligand, the fluorescence of both MOFs can similarly be assigned to intraligand $^1\pi\pi^*$ and $^1n\pi^*$ transitions. The relatively small variation of *ca.* 19 nm in the emission maxima of the two MOFs can possibly be assigned to the different charge density of the coordinated Ca^{2+} and Sr^{2+} ions and to the different conformation of the fluorophores in **1** and **2** [51,64]. As we can see in the crystal structure of **2**, only one type of ligand exists, in contrast to the case **1** where the ligand exists in three different conformations with torsion angles between amino groups of 62.7°, 69.4° and 130.5°.

3.4. Fluorescence quenching by volatile aldehydes

Volatile aldehydes such as acetaldehyde are widely used in the chemical industry as precursors to pyridine derivatives and various polymers and constitute an important class of organic pollutants known for their toxicity and carcinogenicity even at low exposure levels [74,75]. For example, acetaldehyde is classified as toxic and possibly carcinogenic upon long term workplace exposure and has a threshold limit value (TLV) of 25 ppm [76]. Therefore, there is always a need for the development of new sensors which can rapidly and reliably detect and quantify aldehyde vapors. Luminescent MOFs are emerging as a new highly promising class of fluorescent sensory materials due to their ease of functionalization combined with their porosity and diverse emission properties [22,77–80]. However, even though there is a plethora of examples where MOFs act as sensors in liquid media, sensing of gas phase analytes by MOFs remains relatively rare [81,82].

The fact that both MOFs **1** and **2** possess three dimensional structures which contain uncoordinated amino groups which are highly reactive towards aldehydes, motivated us to investigate if they can interact with gas phase aldehydes thereby providing a possible means for their detection. Thus, small quantities of crystals of **1** and **2** were immobilized on a side window of a standard 3.5 mL quartz fluorescence cuvette and their fluorescence spectra were recorded. Subsequently, a small amount (50 μL) of the tested aldehyde (acetaldehyde, propionaldehyde and isobutylaldehyde) was placed with the use of a microsyringe at the bottom of the cuvette taking care that the liquid does not come to direct contract with the crystals of **1** and **2** and the cuvette was firmly capped thereby creating a chamber saturated with the vapors of the tested aldehyde [83]. The emission spectra were recorded over a period of 45 min. Fig. 6 displays the time-dependent emission spectra of **1** and **2** in the presence acetaldehyde vapors. Upon exposure to acetaldehyde vapors the emission of **1** is instantly quenched by more than 75% of its original intensity and by 81% after 45 min (Fig. 6A) while the emission of **2** is quenched by 74% with a concomitant modest red shift of *ca.* 17 nm (Fig. 6B).

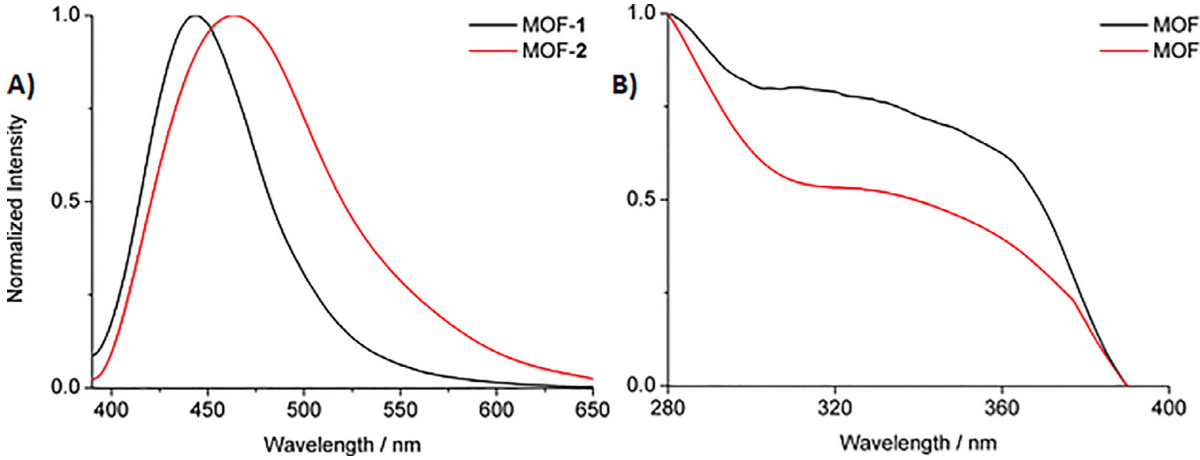

Fig. 5. Solid state (A) emission (λ_{exc} = 350 nm) and (B) excitation spectra of **1** and **2** at room-temperature.

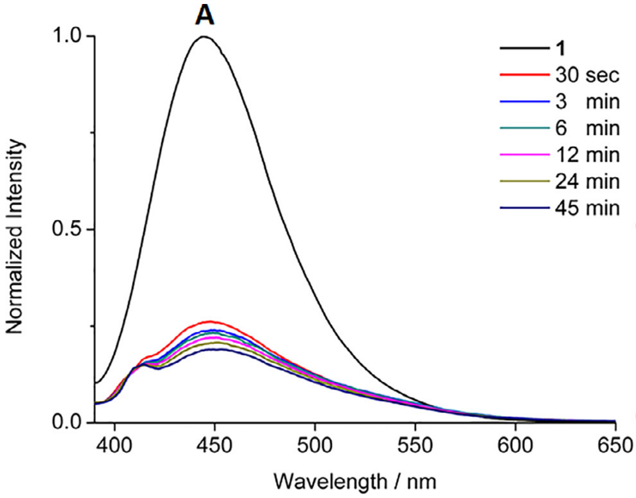

Fig. 6. Emission spectra over time of (A) **1** and (B) **2** upon exposure to acetaldehyde vapors (λ_{ex} = 370 nm).

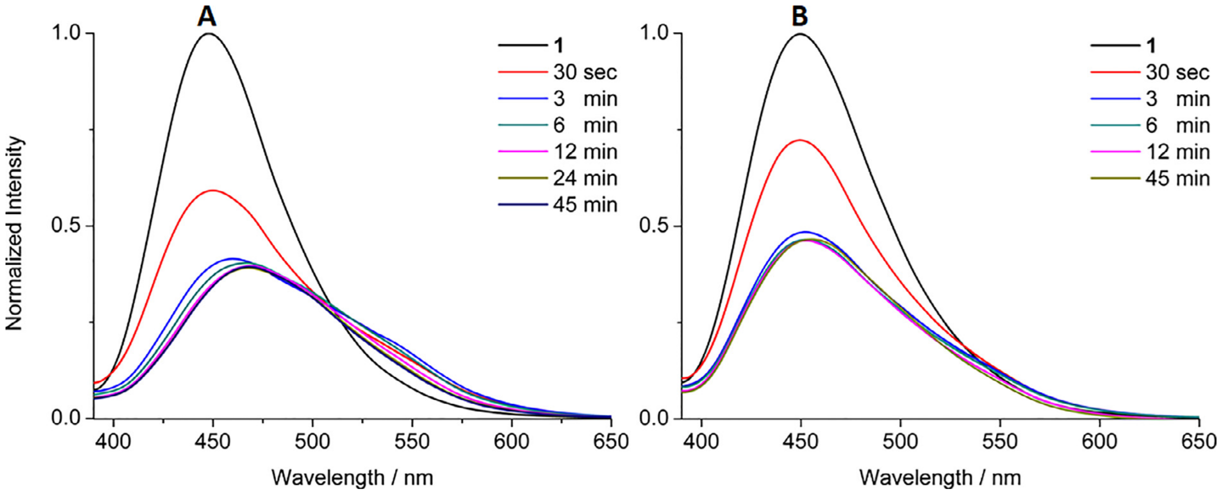

Fig. 7. Emission spectra over time of **1** upon exposure to (A) propionaldehyde and (B) isobutylaldehyde vapors (λ_{ex} = 370 nm).

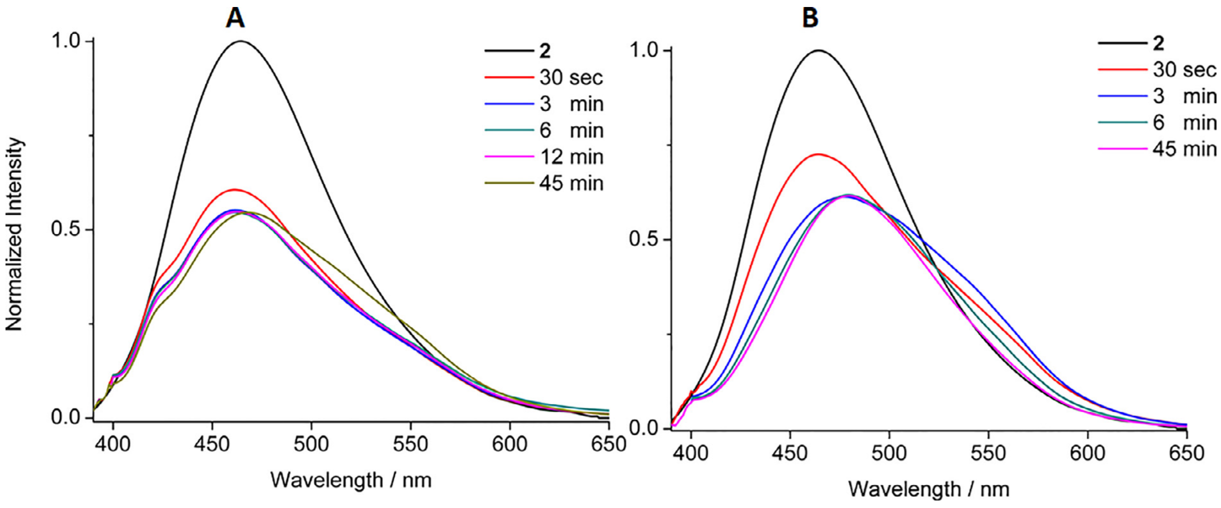

Fig. 8. Emission spectra over time of **2** upon exposure to (A) propionaldehyde and (B) isobutylaldehyde vapors (λ_{ex} = 370 nm).

To evaluate the sensing ability of **1** and **2** towards other volatile aldehydes we performed additional sensing experiments using this time propionaldehyde and isobutylaldehyde. As seen in Fig. 7A the presence of propionaldehyde for 6 min leads to a significant loss of the initial emission intensity of **1** by *ca.* 59% and a concomitant red-shift of 16 nm; reaching equilibrium after a period of 12 min, while isobutyldehyde leads to a decrease of 53% of signal intensity (Fig. 7B). Very similar fluorescence quenching occurs in the case of **2**. Fig. 8 presents the fluorescence spectra of **2** upon exposure to propionaldehyde (Fig. 8A) and isobutaldehyde (Fig. 8B). It was found that the original emission intensity was quenched by 45% and 39% respectively. It can generally be observed that **1** and **2** show a significantly more pronounced response towards acetaldehyde both in terms of kinetics and total quenching percentage in comparison to propionaldehyde and isobutaldehyde. This difference may be attributed to the smaller molecular size and the greater volatility of acetaldehyde in comparison to its bulkier counterparts.

As shown in the Fig. S6, the aldehydes exhibit a strong absorption from 240 to 330 nm, with virtually no absorption at the excitation wavelength of 370 nm. Additionally, their absorption spectra do not show any overlap with the absorption band of neither of the MOFs (Fig. S7). Hence, the observed fluorescence quenching cannot be attributed to a competitive absorption mechanism (inner filter effect). However it must be noted that both **1** and **2** have relatively small solvent accessible voids and small channels (*vide supra*), which indicate that the sorption of aldehydes is probably taking place principally on the surface of the MOFs. In future studies planned in our group, it will be interesting to evacuate the pore space of **1** and **2** and also prepare similar MOFs with larger channels and voids in order to further enhance the sorption and sensing of aldehydes.

4. Conclusion

In summary, two new alkaline earth metal ion MOFs with the H_2bpdc-$(NH_2)_2$ ligand were isolated. Both MOFs showed three dimensional structures and displayed interesting structural features and diverse structural topologies. **1** and **2** exhibit ligand based bright blue fluorescence at room temperature in the solid state. Moreover, both MOFs showed encouraging preliminary results as fluorescent sensors for gas phase aldehydes which prompts us to conduct further investigations. Research on development new AEMOF based sensors for aldehydes and other volatile organic compounds are underway in our group.

Appendix A. Supplementary data

CCDC 1833862–1833863 contains the supplementary crystallographic data for this paper. These data can be obtained free of charge via http://www.ccdc.cam.ac.uk/conts/retrieving.html, or from the Cambridge Crystallographic Data Centre, 12 Union Road, Cambridge CB2 1EZ, UK; fax: (+44) 1223-336-033; or e-mail: deposit@ccdc.cam.ac.uk. Supplementary data associated with this article can be found, in the online version, at https://doi.org/10.1016/j.poly.2018.07.010.

References

[1] H.-C. Zhou, J.R. Long, O.M. Yaghi, Introduction to metal-organic frameworks, Chem. Rev. 112 (2012) 673–674.

[2] M. O'Keeffe, O.M. Yaghi, Deconstructing the crystal structures of metal-organic frameworks and related materials into their underlying nets, Chem. Rev. 112 (2012) 675–702.

[3] H. Furukawa, K.E. Cordova, M. O'Keeffe, O.M. Yaghi, The chemistry and applications of metal-organic frameworks, Science 341 (2013) 1230444.

[4] M. Eddaoudi, J. Kim, N. Rosi, D. Vodak, J. Wachter, M. O'Keeffe, O.M. Yaghi, Systematic design of pore size and functionality in isoreticular MOFs and their application in methane storage, Science 295 (2002) 469–472.

[5] H. Li, K. Wang, Y. Sun, C.T. Lollar, J. Li, H.-C. Zhou, Recent advances in gas storage and separation using metal–organic frameworks, Mater. Today 21 (2018) 108–121.

[6] D. Alezi, Y. Belmabkhout, M. Suyetin, P.M. Bhatt, Ł.J. Weseliński, V. Solovyeva, K. Adil, I. Spanopoulos, P.N. Trikalitis, A.-H. Emwas, M. Eddaoudi, MOF crystal chemistry paving the way to gas storage needs: aluminum-based soc-MOF for CH4, O2, and CO2 storage, J. Am. Chem. Soc. 137 (2015) 13308–13318.

[7] J.-M. Lin, C.-T. He, Y. Liu, P.-Q. Liao, D.-D. Zhou, J.-P. Zhang, X.-M. Chen, A metal-organic framework with a pore size/shape suitable for strong binding and close packing of methane, Angew. Chem. Int. Ed. 55 (2016) 4674–4678.

[8] J.A. Mason, M. Veenstra, J.R. Long, Evaluating metal-organic frameworks for natural gas storage, Chem. Sci. 5 (2014) 32–51.

[9] D. Zhao, D. Yuan, A. Yakovenko, H.-C. Zhou, A NbO-type metal-organic framework derived from a polyyne-coupled di-isophthalate linker formed in situ, Chem. Commun. 46 (2010) 4196–4198.

[10] Z. Bao, G. Chang, H. Xing, R. Krishna, Q. Ren, B. Chen, Potential of microporous metal-organic frameworks for separation of hydrocarbon mixtures, Energy Environ.. Sci. 9 (2016) 3612–3641.

[11] J. Liu, L. Chen, H. Cui, J. Zhang, L. Zhang, C.Y. Su, Applications of metal-organic frameworks in heterogeneous supramolecular catalysis, Chem. Soc. Rev. 43 (2014) 6011–6061.

[12] V.P. Santos, T.A. Wezendonk, J.J.D. Jaén, A.I. Dugulan, M.A. Nasalevich, H.-U. Islam, A. Chojecki, S. Sartipi, X. Sun, A.A. Hakeem, A.C.J. Koeken, M. Ruitenbeek, T. Davidian, G.R. Meima, G. Sankar, F. Kapteijn, M. Makkee, J. Gascon, Metal organic framework-mediated synthesis of highly active and stable Fischer-Tropsch catalysts, Nat. Commun. 6 (2015) 6451.

[13] M. Zhao, S. Ou, C.-D. Wu, Porous metal-organic frameworks for heterogeneous biomimetic catalysis, Acc. Chem. Res. 47 (2014) 1199–1207.

[14] S. Rapti, D. Sarma, S.A. Diamantis, E. Skliri, G.S. Armatas, A.C. Tsipis, Y.S. Hassan, M. Alkordi, C.D. Malliakas, M.G. Kanatzidis, T. Lazarides, J.C. Plakatouras, M.J. Manos, All in one porous material: exceptional sorption and selective sensing of hexavalent chromium by using a Zr4+ MOF, J. Mater. Chem. A 5 (2017) 14707–14719.

[15] S. Rapti, A. Pournara, D. Sarma, I.T. Papadas, G.S. Armatas, A.C. Tsipis, T. Lazarides, M.G. Kanatzidis, M.J. Manos, Selective capture of hexavalent chromium from an anion-exchange column of metal organic resin-alginic acid composite, Chem. Sci. 7 (2016) 2427–2436.

[16] L. Zhu, D. Sheng, C. Xu, X. Dai, M.A. Silver, J. Li, P. Li, Y. Wang, Y. Wang, L. Chen, C. Xiao, J. Chen, R. Zhou, C. Zhang, O.K. Farha, Z. Chai, T.E. Albrecht-Schmitt, S. Wang, Identifying the recognition site for selective trapping of (99)TcO4(-) in a hydrolytically stable and radiation resistant cationic metal-organic framework, J. Am. Chem. Soc. 139 (2017) 14873–14876.

[17] B. Li, Y. Zhang, D. Ma, Z. Shi, S. Ma, Mercury nano-trap for effective and efficient removal of mercury(II) from aqueous solution, Nat. Commun. 5 (2014) 5537.

[18] R. Ricco, K. Konstas, M.J. Styles, J.J. Richardson, R. Babarao, K. Suzuki, P. Scopece, P. Falcaro, Lead(ii) uptake by aluminium based magnetic framework composites (MFCs) in water, J. Mater. Chem. A 3 (2015) 19822–19831.

[19] F. Luo, J.L. Chen, L.L. Dang, W.N. Zhou, H.L. Lin, J.Q. Li, S.J. Liu, M.B. Luo, High-performance Hg2+ removal from ultra-low-concentration aqueous solution using both acylamide- and hydroxyl-functionalized metal-organic framework, J. Mater. Chem. A 3 (2015) 9616–9620.

[20] K.-K. Yee, N. Reimer, J. Liu, S.-Y. Cheng, S.-M. Yiu, J. Weber, N. Stock, Z. Xu, Effective mercury sorption by thiol-laced metal-organic frameworks: in strong acid and the vapor phase, J. Am. Chem. Soc. 135 (2013) 7795–7798.

[21] Y.-S. Wei, X.-P. Hu, Z. Han, X.-Y. Dong, S.-Q. Zang, T.C.W. Mak, Unique proton dynamics in an efficient MOF-based proton conductor, J. Am. Chem. Soc. 139 (2017) 3505–3512.

[22] M.D. Allendorf, C.A. Bauer, R.K. Bhakta, R.J.T. Houk, Luminescent metal-organic frameworks, Chem. Soc. Rev. 38 (2009) 1330–1352.

[23] L.V. Meyer, F. Schonfeld, K. Muller-Buschbaum, Lanthanide based tuning of luminescence in MOFs and dense frameworks – from mono- and multimetal systems to sensors and films, Chem. Commun. 50 (2014) 8093–8108.

[24] Q. Zhang, J. Su, D.W. Feng, Z.W. Wei, X.D. Zou, H.C. Zhou, Piezofluorochromic metal-organic framework: a microscissor lift, J. Am. Chem. Soc. 137 (2015) 10064–10067.

[25] C.Y. Sun, X.L. Wang, X. Zhang, C. Qin, P. Li, Z.M. Su, D.X. Zhu, G.G. Shan, K.Z. Shao, H. Wu, J. Li, Efficient and tunable white-light emission of metal-organic frameworks by iridium-complex encapsulation, Nat. Commun. 4 (2013) 2717.

[26] X.G. Yang, D.P. Yan, Long-afterglow metal-organic frameworks: reversible guest-induced phosphorescence tunability, Chem. Sci. 7 (2016) 4519–4526.

[27] Y.S. Yang, K.Z. Wang, D.P. Yan, Lanthanide doped coordination polymers with tunable afterglow based on phosphorescence energy transfer, Chem. Commun. 53 (2017) 7752–7755.

[28] C.-Y. Sun, X.-L. Wang, X. Zhang, C. Qin, P. Li, Z.-M. Su, D.-X. Zhu, G.-G. Shan, K.-Z. Shao, H. Wu, J. Li, Efficient and tunable white-light emission of metal–organic frameworks by iridium-complex encapsulation, Nat. Commun. 4 (2013) 2717.

[29] L. Zeng, X.Y. Guo, C. He, C.Y. Duan, Metal-organic frameworks: versatile materials for heterogeneous photocatalysis, Acs Catal. 6 (2016) 7935–7947.

[30] A. Dhakshinamoorthy, A.M. Asiri, H. Garcia, Metal-organic framework (MOF) compounds: photocatalysts for redox reactions and solar fuel production, Angew. Chem. Int. Ed. 55 (2016) 5414–5445.

[31] Y.B. Huang, J. Liang, X.S. Wang, R. Cao, Multifunctional metal-organic framework catalysts: synergistic catalysis and tandem reactions, Chem. Soc. Rev. 46 (2017) 126–157.

[32] C. Gao, J. Wang, H.X. Xu, Y.J. Xiong, Coordination chemistry in the design of heterogeneous photocatalysts, Chem. Soc. Rev. 46 (2017) 2799–2823.

[33] H. Assi, G. Mouchaham, N. Steunou, T. Devic, C. Serre, Titanium coordination compounds: from discrete metal complexes to metal-organic frameworks, Chem. Soc. Rev. 46 (2017) 3431–3452.

[34] A. Dhakshinamoorthy, A.M. Asiri, H. García, Metal-organic framework (MOF) compounds: photocatalysts for redox reactions and solar fuel production, Angew. Chem. Int. Ed. 55 (2016) 5414–5445.

[35] Y. Zhou, B. Yan, Ratiometric detection of temperature using responsive dual-emissive MOF hybrids, J. Mater. Chem. C 3 (2015) 9353–9358.

[36] J. Rocha, C.D.S. Brites, L.D. Carlos, Lanthanide organic framework luminescent thermometers, Chem. – A Eur. J. 22 (2016) 14782–14795.

[37] D. Zhao, X. Rao, J. Yu, Y. Cui, Y. Yang, G. Qian, Design and synthesis of an MOF thermometer with high sensitivity in the physiological temperature range, Inorg. Chem. 54 (2015) 11193–11199.

[38] J. Della Rocca, D.M. Liu, W.B. Lin, Nanoscale metal-organic frameworks for biomedical imaging and drug delivery, Acc. Chem. Res. 44 (2011) 957–968.

[39] I. Martinic, S.V. Eliseeva, S. Petoud, Near-infrared emitting probes for biological imaging: organic fluorophores, quantum dots, fluorescent proteins, lanthanide (III) complexes and nanomaterials, J. Lumin. 189 (2017) 19–43.

[40] S. Petoud, A. Foucault-Collet, S.V. Eliseeva, K.A. Gogick, K.A. White, I. Nazarenko, V. Placide, S. Villette, N.L. Rosi, Near-infrared emitting lanthanide complexes for optical imaging applications in biology: polymetallic dendrimers and metal-organic frameworks, J. Biol. Inorg. Chem. 19 (2014), S736-S736.

[41] E. Evangelio, A. Yazdi, A. Carne, I. Imaz, D. Maspoch, K. White, D. Chengelis, K. Gogick, N. Rosi, E. Evangelio, A. Foucault, S. Eliseeva, S. Petoud, NIR emitting lanthanide nanoscale MOFs for biological imaging, J. Biol. Inorg. Chem. 19 (2014), S441-S441.

[42] A. Foucault-Collet, K.A. Gogick, K.A. White, S. Villette, A. Pallier, G. Collet, C. Kieda, T. Li, S.J. Geib, N.L. Rosi, S. Petoud, Lanthanide near infrared imaging in living cells with Yb3+ nano metal organic frameworks, Proc. Natl. Acad. Sci. USA 110 (2013) 17199–17204.

[43] L. Chen, J.-W. Ye, H.-P. Wang, M. Pan, S.-Y. Yin, Z.-W. Wei, L.-Y. Zhang, K. Wu, Y.-N. Fan, C.-Y. Su, Ultrafast water sensing and thermal imaging by a metal-organic framework with switchable luminescence, Nat. Commun. 8 (2017) 15985.

[44] T. Xia, T. Song, G. Zhang, Y. Cui, Y. Yang, Z. Wang, G. Qian, A terbium metal-organic framework for highly selective and sensitive luminescence sensing of Hg2+ ions in aqueous solution, Chem. – A Eur. J. 22 (2016) 18429–18434.

[45] G. Ji, J. Liu, X. Gao, W. Sun, J. Wang, S. Zhao, Z. Liu, A luminescent lanthanide MOF for selectively and ultra-high sensitively detecting Pb2+ ions in aqueous solution, J. Mater. Chem. A 5 (2017) 10200–10205.

[46] W.P. Lustig, S. Mukherjee, N.D. Rudd, A.V. Desai, J. Li, S.K. Ghosh, Metal-organic frameworks: functional luminescent and photonic materials for sensing applications, Chem. Soc. Rev. 46 (2017) 3242–3285.

[47] Z. Hu, B.J. Deibert, J. Li, Luminescent metal-organic frameworks for chemical sensing and explosive detection, Chem. Soc. Rev. 43 (2014) 5815–5840.

[48] F.-Y. Yi, D. Chen, M.-K. Wu, L. Han, H.-L. Jiang, Chemical sensors based on metal-organic frameworks, ChemPlusChem 81 (2016) 675–690.

[49] J.-N. Hao, B. Yan, A water-stable lanthanide-functionalized MOF as a highly selective and sensitive fluorescent probe for Cd2+, Chem. Commun. 51 (2015) 7737–7740.

[50] E. Papazoi, A. Douvali, S. Rapti, E. Skliri, G.S. Armatas, G.S. Papaefstathiou, X. Wang, Z.-F. Huang, S. Kaziannis, C. Kosmidis, A.G. Hatzidimitriou, T. Lazarides, M.J. Manos, A microporous Mg2+ MOF with cation exchange properties in a single-crystal-to-single-crystal fashion, Inorg. Chem. Front. 4 (2017) 530–536.

[51] Z.H. Fard, Y. Kalinovskyy, D.M. Spasyuk, B.A. Blight, G.K.H. Shimizu, Alkaline-earth phosphonate MOFs with reversible hydration-dependent fluorescence, Chem. Commun. 52 (2016) 12865–12868.

[52] X.-Y. Dong, X.-P. Hu, H.-C. Yao, S.-Q. Zang, H.-W. Hou, T.C.W. Mak, Alkaline earth metal (Mg, Sr, Ba)–organic frameworks based on 2,2′,6,6′-tetracarboxybiphenyl for proton conduction, Inorg. Chem. 53 (2014) 12050–12057.

[53] A. Margariti, S. Rapti, A.D. Katsenis, T. Friscic, Y. Georgiou, M.J. Manos, G.S. Papaefstathiou, Cu2+ sorption from aqueous media by a recyclable Ca2+ framework, Inorg. Chem. Front. 4 (2017) 773–781.

[54] Y. Hou, J. Sun, D. Zhang, D. Qi, J. Jiang, Porphyrin-alkaline earth MOFs with the highest adsorption capacity for methylene blue, Chemistry 22 (2016) 6345–6352.

[55] Z.-F. Wu, B. Tan, M.-L. Feng, A.-J. Lan, X.-Y. Huang, A magnesium MOF as a sensitive fluorescence sensor for CS2 and nitroaromatic compounds, J. Mater. Chem. A 2 (2014) 6426–6431.

[56] A.E. Platero-Prats, N. Snejko, M. Iglesias, Á. Monge, E. Gutiérrez-Puebla, Insight into Lewis acid catalysis with alkaline-earth MOFs: the role of polyhedral symmetry distortions, Chem. – A Eur. J. 19 (2013) 15572–15582.

[57] A. Mallick, B. Garai, M.A. Addicoat, P.S. Petkov, T. Heine, R. Banerjee, Solid state organic amine detection in a photochromic porous metal organic framework, Chem. Sci. 6 (2015) 1420–1425.

[58] K. Sumida, M.R. Hill, S. Horike, A. Dailly, J.R. Long, Synthesis and hydrogen storage properties of Be12(OH)12(1,3,5-benzenetribenzoate)4, J. Am. Chem. Soc. 131 (2009) 15120–15121.

[59] M. Kang, D. Luo, Z. Lin, G. Thiele, S. Dehnen, Crystalline beryllium carboxylate frameworks containing inorganic chains of BeO4 tetrahedra, CrystEngComm 15 (2013) 1845–1848.

[60] R.M.P. Colodrero, P. Olivera-Pastor, E.R. Losilla, D. Hernández-Alonso, M.A.G. Aranda, L. Leon-Reina, J. Rius, K.D. Demadis, B. Moreau, D. Villemin, M. Palomino, F. Rey, A. Cabeza, High proton conductivity in a flexible, cross-linked, ultramicroporous magnesium tetraphosphonate hybrid framework, Inorg. Chem. 51 (2012) 7689–7698.

[61] H. Deng, S. Grunder, K.E. Cordova, C. Valente, H. Furukawa, M. Hmadeh, F. Gandara, A.C. Whalley, Z. Liu, S. Asahina, H. Kazumori, M. O'Keeffe, O. Terasaki, J.F. Stoddart, O.M. Yaghi, Large-pore apertures in a series of metal-organic frameworks, Science 336 (2012) 1018–1023.

[62] A.M. Fracaroli, H. Furukawa, M. Suzuki, M. Dodd, S. Okajima, F. Gándara, J.A. Reimer, O.M. Yaghi, Metal-organic frameworks with precisely designed interior for carbon dioxide capture in the presence of water, J. Am. Chem. Soc. 136 (2014) 8863–8866.

[63] A. Douvali, A.C. Tsipis, S.V. Eliseeva, S. Petoud, G.S. Papaefstathiou, C.D. Malliakas, I. Papadas, G.S. Armatas, I. Margiolaki, M.G. Kanatzidis, T. Lazarides, M.J. Manos, Turn-on luminescence sensing and real-time detection of traces of water in organic solvents by a flexible metal-organic framework, Angew. Chem. Int. Ed. 54 (2015) 1651–1656.

[64] A. Douvali, G.S. Papaefstathiou, M.P. Gullo, A. Barbieri, A.C. Tsipis, C.D. Malliakas, M.G. Kanatzidis, I. Papadas, G.S. Armatas, A.G. Hatzidimitriou, T. Lazarides, M.J. Manos, Alkaline earth metal ion/dihydroxy–terephthalate MOFs: structural diversity and unusual luminescent properties, Inorg. Chem. 54 (2015) 5813–5826.

[65] A. Schoedel, M. Li, D. Li, M. O'Keeffe, O.M. Yaghi, Structures of metal-organic frameworks with rod secondary building units, Chem. Rev. 116 (2016) 12466–12535.

[66] I.A. Bruker Analytical X-ray Systems, Version 2 User Manual, M86–E01078 2006 Madison, WI.

[67] I.S.A.-D.A.C.M. Siemens Industrial Automation, WI, 1996.

[68] J.R.C.P.W. Betteridge, R.I. Cooper, K. Prout, D.J. Watkin, J. Appl. Cryst. 36 (2003) 1487.

[69] G.J.C.L. Palatinus, Appl. Cryst. 40 (2007) 786–790.

[70] C.F. Macrae, P.R. Edgington, P. McCabe, E. Pidcock, G.P. Shields, R. Taylor, M. Towler, J. van De Streek, Mercury: visualization and analysis of crystal structures, J. Appl. Crystallogr. 39 (2006) 453–457.

[71] N.L. Rosi, J. Kim, M. Eddaoudi, B. Chen, M. O'Keeffe, O.M. Yaghi, Rod packings and metal–organic frameworks constructed from rod-shaped secondary building units, J. Am. Chem. Soc. 127 (2005) 1504–1518.

[72] C. Serre, F. Millange, C. Thouvenot, M. Noguès, G. Marsolier, D. Louër, G. Férey, Very large breathing effect in the first nanoporous chromium(III)-based solids: MIL-53 or CrIII(OH)·{O2C–C6H4–CO2}·{HO2C–C6H4–CO2H}x·H2Oy, J. Am. Chem. Soc. 124 (2002) 13519–13526.

[73] K. Barthelet, J. Marrot, D. Riou, G. Férey, A Breathing hybrid organic-inorganic solid with very large pores and high magnetic characteristics, Angew. Chem. Int. Ed. 41 (2002) 281–284.

[74] M.S. Kamal, S.A. Razzak, M.M. Hossain, Catalytic oxidation of volatile organic compounds (VOCs) – a review, Atmos. Environ. 140 (2016) 117–134.

[75] P. Aragon, J. Atienza, M.D. Climent, Analysis of organic compounds in air: a review, Crit. Rev. Anal. Chem. 30 (2000) 121–151.

[76] M. Eckert, G. Fleischmann, R. Jira, H.M. Bolt, K. Golka, Acetaldehyde, in: Ullmann's Encyclopedia of Industrial Chemistry, 2006.

[77] L.E. Kreno, K. Leong, O.K. Farha, M. Allendorf, R.P. Van Duyne, J.T. Hupp, Metal-organic framework materials as chemical sensors, Chem. Rev. 112 (2012) 1105–1125.

[78] A. Chidambaram, K.C. Stylianou, Electronic metal-organic framework sensors, Inorg. Chem. Front. 5 (2018) 979–998.

[79] S.A. Diamantis, A. Margariti, A.D. Pournara, G.S. Papaefstathiou, M.J. Manos, T. Lazarides, Luminescent metal-organic frameworks as chemical sensors: common pitfalls and proposed best practices, Inorg. Chem. Front. (2018), https://doi.org/10.1039/C1038QI00090E.

[80] P. Kumar, A. Deep, K.-H. Kim, Metal organic frameworks for sensing applications, TrAC Trends Anal. Chem. 73 (2015) 39–53.

[81] S.L. Jackson, A. Rananaware, C. Rix, S.V. Bhosale, K. Latham, Highly fluorescent metal-organic framework for the sensing of volatile organic compounds, Cryst. Growth Des. 16 (2016) 3067–3071.

[82] X.-G. Liu, H. Wang, B. Chen, Y. Zou, Z.-G. Gu, Z. Zhao, L. Shen, A luminescent metal-organic framework constructed using a tetraphenylethene-based ligand for sensing volatile organic compounds, Chem. Commun. 51 (2015) 1677–1680.

[83] C. Wang, W. Lin, Diffusion-controlled luminescence quenching in metal–organic frameworks, J. Am. Chem. Soc. 133 (2011) 4232–4235.